Lattice dynamics of α-AlH$_3$ and α-AlD$_3$ by inelastic neutron scattering: High-energy band of optical bond-stretching vibrations

A. I. Kolesnikov,[1,*] V. E. Antonov,[2] Yu. E. Markushkin,[3] I. Natkaniec,[4] and M. K. Sakharov[2]

[1]*Intense Pulsed Neutron Source Division, Argonne National Laboratory, Argonne, Illinois 60439, USA*
[2]*Institute of Solid State Physics, RAS, 142432 Chernogolovka, Moscow District, Russia*
[3]*Bochvar All-Russian Scientific Research Institute for Inorganic Materials, Rogova Street 5a, 123060 Moscow, Russia*
[4]*Frank Laboratory of Neutron Physics, Joint Institute for Nuclear Research, 141980 Dubna, Moscow District, Russia*
and H. Niewodniczanski Institute of Nuclear Physics, PAS, 31-342 Krakow, Poland

Inelastic neutron scattering (INS) spectra of trigonal α-AlH$_3$ and α-AlD$_3$ have been measured in a wide range (5–150 meV) of energy transfers with a much better statistical accuracy than previously using the inverted-geometry NERA-PR spectrometer at JINR, Dubna. The studied energy interval covers the range of low-frequency lattice vibrations and a broad band of optical H vibrations. By using a direct-geometry HRMECS spectrometer at ANL, Argonne, the AlH$_3$ hydride was also examined by INS at energy transfers up to 315 meV in the regime of small momentum transfers. This significantly enhanced the contribution from the one-phonon neutron scattering and allowed an observation and accurate examination of one more, high-energy band of optical H vibrations predicted theoretically [C. Wolverton *et al.*, Phys. Rev. B **69**, 144109 (2004)]. Combining the obtained experimental data, the entire spectrum of phonon density of states was reconstructed for both α-AlH$_3$ and α-AlD$_3$.

PACS number(s): 63.20.Dj, 63.20.Pw, 78.70.Nx

I. INTRODUCTION

The 12-layer trigonal crystal structure of α-AlH$_3$ (space group $R\bar{3}m$) consists of equally spaced alternating planes of Al and H atoms stacked perpendicular to the c axis.[1] Columns of Al atoms and spirals of H atoms are parallel to the c axis and form a three-dimensional network of Al-H-Al bridges. Any hydrogen atom in aluminum trihydride has only two nearest Al neighbors and does not occupy any symmetrical interstitial position in the metal sublattice as it does in most other hydrides.

Earlier,[2] we studied the vibrational spectrum of α-AlH$_3$ at 25 K by inelastic neutron scattering (INS) with a very good energy resolution of $\Delta E / E \leqslant 2\%$ using the inverse-geometry time-focused crystal analyzer (TFXA) spectrometer at ISIS, UK. In order to better understand some characteristic features of the AlH$_3$ spectrum, we also measured, though only in the rough, the INS spectrum of α-AlD$_3$ using the inverse-geometry KDSOG-M spectrometer at JINR in Dubna, Russia. The obtained data allowed us to reliably determine the contribution of one-phonon neutron scattering to the INS spectrum of AlH$_3$ at energy transfers up to 150 meV and to identify the range (0–42 meV) of lattice vibrational modes and the range (62–131 meV) of hydrogen optical modes.

Recently,[3,4] the phonon density of states was calculated for α-AlH$_3$ using the density-functional theory. The calculations reproduced the experimental band of low-frequency lattice vibrations at energies below 50 meV (three acoustic and three optical branches) and the broad band of optical H vibrations between 55 and 130 meV (rotational motions and H–Al–H bond-bending deformations of corner-sharing AlH$_6$ octahedra; 12 modes in total). Additionally, these calculations predicted the occurrence of one more H optical band composed of two broad peaks centered near 208 and 231 meV (six modes of Al–H bond-stretching motions of H atoms).[3]

In the experimental INS spectrum of AlH$_3$,[2] the one-phonon scattering intensity was efficiently suppressed at energy transfers exceeding 150 meV and it could not be reliably isolated from the intense multiphonon contribution. The drastic weakening of the one-phonon scattering intensity was caused by the rapid decrease in the Debye-Waller factor, $\exp(-\langle u^2 \rangle Q^2)$, with increasing energy transfer due to the combined effect of the large mean-squared displacement $\langle u^2 \rangle$ of the H atoms and the large neutron momentum transfers Q at high-energy transfers. The latter is intrinsic to inverse-geometry spectrometers that have small final neutron energy of about 4 meV.

In the present paper, the INS spectrum of α-AlH$_3$ was measured at 10 K using a direct-geometry high-resolution medium energy chopper spectrometer (HRMECS) at ANL. With the HRMECS, the squared neutron momentum transfers in the energy range 150–315 meV were decreased by a factor of 5 compared to the inverse-geometry spectrum measured in Ref. 2. Due to the large value of $\langle u^2 \rangle$ of the H atoms, this significantly enhanced the contribution of the one-phonon scattering and allowed an accurate examination of the new band of Al-H stretching modes. The INS spectra of α-AlH$_3$ at 9 and 291 K and the spectrum of α-AlD$_3$ at 9 K were also measured using the inverse-geometry NERA-PR spectrometer at JINR. The measurements were mainly aimed at examining the harmonicity of the AlH$_3$ spectrum and reproducibility of its fine structure at energy transfers below 150 meV.

II. EXPERIMENTAL DETAILS AND DATA TREATMENT

Powder samples of α-AlH$_3$ and α-AlD$_3$ were prepared using the same techniques as in Ref. 2. The AlH$_3$ powder with a grain size of 30 μm and a purity of 99.8 wt. % was produced by a reaction of LiAlH$_4$ with AlCl$_3$ in ether solu-

tion at room temperature.[5] The AlD$_3$ powder with a grain size of 20 μm was prepared in the same way using the deuterium-substituted reagents. The main impurity in the deuteride was protium and the H/(H+D) atomic ratio made up 1.5±0.5% according to the spectral analysis.

A 2 g sample of AlH$_3$ was measured by INS at 10 K with the direct-geometry HRMECS,[6] which uses monochromatic incident neutrons. The energy E_i of the incident neutrons is selected with a rotating Fermi chopper, and the scattered neutrons are registered in a wide range of scattering angles of ϑ from −20° to 132°. Using high E_i and small ϑ decreases the neutron momentum transfer concomitant with any given energy transfer. In the present experiment, we used E_i=50, 200, and 355 meV. The measuring time at each E_i was one day. The energy resolution $\Delta E/E_i$ varied approximately linearly from 3% to 2% in the range of energy transfers from $E_i/2$ to E_i.

INS spectra of a 4 g sample of AlH$_3$ and a 30 g sample of AlD$_3$ were also measured with the inverse-geometry time-of-flight NERA-PR spectrometer[7] at 15 scattering angles ranging from 20° to 160°. The energy E_i of the incident neutrons was determined from their time of flight using a path length of 109.05 m between the neutron moderator and the sample. The energy of the registered inelastically scattered neutrons was fixed at an average value of 4.5 meV using a cold beryllium filter and pyrolytic-graphite analyzers. The AlH$_3$ sample was measured for 8 h at 9 and 291 K; AlD$_3$ sample for 12 h at 9 K. At energy transfers below 150 meV, the NERA-PR spectrometer provided nearly the same resolution $\Delta E/E \approx 2\%$ as the TFXA spectrometer.[2]

With both spectrometers, the sample was placed in a flat thin-walled aluminum container. Background spectra from empty containers were measured separately under similar conditions and subtracted from the corresponding raw sample data. The resulting INS data were transformed to the dynamical structure factors $S(Q,E)$, and the multiphonon neutron scattering contributions were calculated in a harmonic isotropic approximation using the iterative technique of Ref. 8. The experimental $S(Q,E)$ spectra and the calculated multiphonon spectra were transformed to the nearly spectrometer-independent, generalized vibrational densities of states, $G(E)$, according to

$$G(E) = \frac{S(Q,E)E}{Q^2[n(E,T)+1]}, \quad (1)$$

where $n(E,T)$ is the Bose factor. Subtracting the multiphonon $G(E)$ spectra from the experimental ones gave one-phonon $G(E)$ spectra. Combining most reliable portions of the one-phonon $G(E)$ spectra obtained with the NERA-PR spectrometer and HRMECS, the phonon density of states $g(E)$ was estimated.

III. RESULTS AND DISCUSSION

A. Studies with the NERA-PR neutron spectrometer

The experimental spectra $G(E)$ of the α-AlH$_3$ and α-AlD$_3$ samples measured with the NERA-PR spectrometer are shown in Figs. 1 and 2(a), respectively. The spectra of both
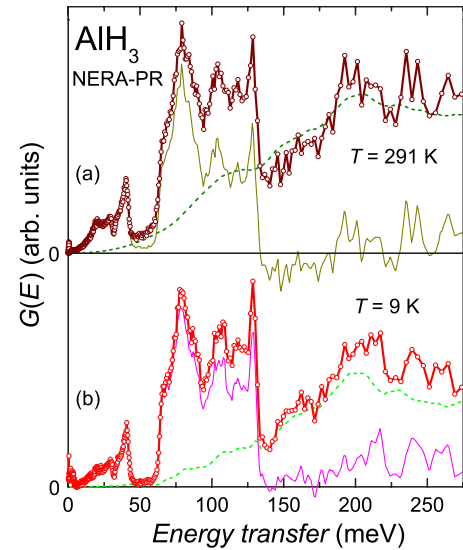
FIG. 1. (Color online) Generalized vibrational density of states $G(E)$ of AlH$_3$ measured at (a) 291 K and (b) 9 K with the NERA-PR spectrometer. The open circles connected with solid lines show the experimental data. The dashed curves present the calculated multiphonon contributions. The lower thin solid curves show the "one-phonon" spectra obtained by subtracting the multiphonon contributions from the corresponding experimental data.

AlH$_3$ and AlD$_3$ mainly represent the inelastic neutron scattering by H and D atoms, respectively, because Al atoms have smaller incoherent (σ^{inc}), coherent (σ^{coh}), and total (σ^{tot}) cross sections of neutron scattering. Namely, σ^{inc}_{Al}=0.01 b, σ^{coh}_{Al}=1.49 b, and σ^{tot}_{Al}=1.50 b, while σ^{inc}_H=80.26 b, σ^{coh}_H=1.76 b, and σ^{tot}_H=82.02 b for hydrogen and σ^{inc}_D=2.05 b, σ^{coh}_D=5.59 b, and σ^{tot}_D=7.64 b for deuterium.[9] In addition, the number of H (D) atoms in AlH$_3$ (AlD$_3$) is three times that of Al atoms.

Compared to the $G(E)$ spectrum of AlH$_3$ measured earlier with the TFXA spectrometer,[2] the spectra measured with the NERA-PR spectrometer have slightly lower energy resolution but much better statistical accuracy at energy transfers $5 < E < 130$ meV. At higher energies, the statistical accuracy and resolution of the NERA-PR data significantly decrease. At energies below 5 meV, the NERA-PR spectra often show spurious intensity.

At energy transfers up to 135 meV, the one-phonon spectrum of AlH$_3$ measured at 9 K [Fig. 1(b)] well reproduces the shape and position of every main feature of the spectrum measured at 25 K in Ref. 2 except for the splitting of the peaklike feature at 118 meV. Most likely, the feature in Ref. 2 looked split due to the insufficient statistical accuracy of the data.

No changes in the shape and position of the main features occurred after heating the AlH$_3$ sample to 291 K [Fig. 1(a)]. This suggests that the corresponding vibrational modes well obey the harmonic behavior at temperatures up to 291 K.

The $G(E)$ spectrum of the AlD$_3$ sample [Fig. 2(a)] is more complex due to the presence of 1.5% hydrogen impurity in the sample. To isolate the contribution from this impurity and to examine the harmonicity of the spectrum with respect to the isotopic substitution of D by H, we fitted the spectrum of
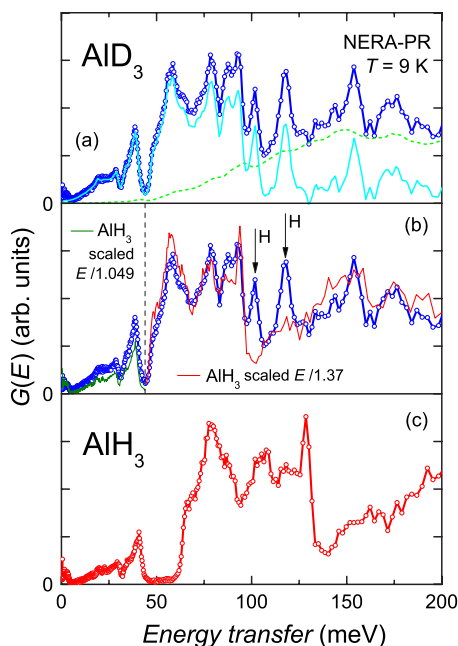
FIG. 2. (Color online) Generalized vibrational densities of states $G(E)$ of AlD$_3$ and AlH$_3$ measured at 9 K with the NERA-PR spectrometer. (a) The open circles connected with solid lines show the experimental data for AlD$_3$. The dashed curve is the calculated multiphonon contribution. The lower thin solid curve is the difference spectrum (the one-phonon contribution). (b) The experimental $G(E)$ of AlD$_3$ from (a) in comparison with the experimental $G(E)$ of AlH$_3$ from (c) plotted with thin solid curves as a function of $E/1.049 \approx E/\sqrt{m_{AlD_3}/m_{AlH_3}}$ at $E<44$ meV and as a function of $E/1.37 \approx E/\sqrt{m_D/m_H}$ at $E>44$ meV. The vertical arrows show the positions of two peaks of local vibrational modes of H impurity in the AlD$_3$ sample.

AlD$_3$ with the experimental spectrum of AlH$_3$ rescaled along the E axis [Fig. 2(b)].

The harmonic isotopic behavior would suggest an inverse proportionality of the vibrational energy E to the square root of the mass m (or the momentum of inertia) of the vibrating (librating) units. The AlH$_3$ spectrum at $E<42$ meV originates from translational vibrations of Al(H$_{1/2}$)$_6$ units of the crystal structure.[2,4,5] As shown in Fig. 2(b) and in more detail in Fig. 3, this low-energy part of the AlH$_3$ spectrum plotted as a function of $E/\sqrt{m_{AlD_3}/m_{AlH_3}} \approx E/\sqrt{33/30} \approx E/1.049$ well describes translational vibrations of Al(D$_{1/2}$)$_6$ units in the AlD$_3$ spectrum. The scaling factor for the optical hydrogen vibrations should be close to $\sqrt{m_D/m_H} \approx \sqrt{2} \approx 1.41$. As seen from Fig. 2(b), the high-energy part of the AlH$_3$ spectrum at $E>60$ meV plotted as a function of $E/1.37 \approx E/\sqrt{2}$ rather well reproduces the energy interval 46–96 meV of the optical D band and its four-peak structure and also the intensity distribution at $E>130$ meV in the AlD$_3$ spectrum. The deviation of the scaling factor from $\sqrt{2}$ may partly result from the stronger interatomic forces in AlD$_3$ compared to those in AlH$_3$ due to the smaller interatomic distances (the lattice parameters are $a=4.431$ Å and $c=11.774$ Å for the deuteride and $a=4.449$ Å and $c=11.804$ Å for the hydride[1]).

The two peaks at 101.5 and 117.5 meV, marked with arrows in the AlD$_3$ spectrum in Fig. 2(b), can be ascribed to
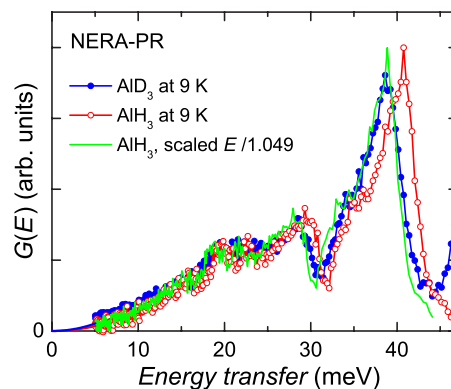
FIG. 3. (Color online) The experimental spectra $G(E)$ of AlD$_3$ (solid circles) and AlH$_3$ (open circles) and the spectrum of AlH$_3$ plotted as a function of $E/1.049 \approx E/\sqrt{m_{AlD_3}/m_{AlH_3}}$ (thin solid line without circles). The rescaled spectrum of AlH$_3$ is normalized to have the same area as the spectrum of AlD$_3$. The unreliable portions of the experimental spectra at $E<5$ meV are interpolated using the Debye approximation $G(E) \propto E^2$.

local defect modes of the hydrogen impurity in the studied AlD$_3$ sample. In fact, the 1.5% H atoms in this sample could not form macroscopic precipitates of AlH$_3$, otherwise an optical H band ranging from 60 to 135 meV [Fig. 2(c)] would have arisen and superimposed onto the band of optical D vibrations, which is not the case. Assuming a random distribution of the 1.5% H atoms over the crystallographically equivalent sites occupied by D and H atoms in the AlD$_3$ sample, the mean distance between the nearest H atoms should be large and the interaction between the H atoms should be small. Each H atom would therefore vibrate nearly independently of others, giving rise to three local defect modes: one mode along the Al–H bond (high-frequency stretching mode) and two modes in the transverse directions (lower-frequency bond-bending modes). The 101.5 and 117.5 meV peaks lie in the range 60–135 meV of the H–Al–H bond-bending modes and could be attributed to the transverse defect modes.

It is worth noting here that the presence of 1.5% H atoms randomly distributed in the AlD$_3$ sample could not noticeably affect the spectrum of low-energy translational vibrations of Al(D$_{1/2}$)$_6$ units (Fig. 3) because of the steep decrease—down to $0.015^6 \approx 10^{-11}$ for the Al(H$_{1/2}$)$_6$ configuration—in the probability for the Al atom to have an increasing number of H neighbors.

B. Studies with the HRMECS neutron spectrometer

Figure 4 shows the $S(Q,E)$ spectra of α-AlH$_3$ measured at $T=10$ K with the HRMECS using the neutrons with the incident energies $E_i=200$ and 355 meV. Two intense and well-resolved peaks centered at 204 and 238 meV are clearly seen in the 355 meV spectrum collected at small scattering angles and, correspondingly, small momentum transfers. The occurrence of two peaks and their positions agree well with the theoretical predictions[3,4] for the phonon band of Al-H bond-stretching motions of H atoms.
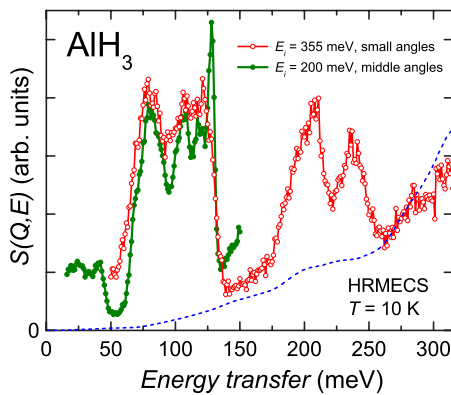
FIG. 4. (Color online) The dynamical structure factor $S(Q,E)$ of AlH$_3$ measured at 10 K with the HRMECS using the neutrons with an incident energy of $E_i=200$ meV (the data are summed over the middle scattering angles 28°–63°) and $E_i=355$ meV (summing over the small angles from −20° to −6° and from +6° to +20°). The dashed curve shows the multiphonon contribution to the 355 meV spectrum calculated using results obtained with $E_i=50$ and 200 meV to construct the $S(Q,E)$ dependence at energy transfers below 135 meV.

The 204 and 238 meV peaks are located deep inside the energy range of multiphonon neutron scattering. To prove that these peaks originated from one-phonon neutron scattering, we analyzed the momentum transfer dependences of the scattering intensity integrated in the vicinity (±20 meV) of the peak maxima and, for comparison, around the nearby point (290 meV) (Fig. 5). Each dependence was fitted with a curve

$$I(Q) = (aQ^2 + bQ^4)\exp(-cQ^2), \qquad (2)$$

where a, b, and c were the fitting parameters. The aQ^2 and bQ^4 factors characterized, respectively, the one and two-phonon scattering contributions. As seen from Fig. 5, the one-phonon contribution dominates in the intensity of both experimental peaks.

The HRMECS spectrum of AlH$_3$ measured using $E_i=200$ meV (Fig. 4) reproduces every detail of the band of optical bond-bending H vibrations in the range 60–135 meV of the NERA-PR spectrum shown in Fig. 1(b). The shape and width of this band in the HRMECS spectrum measured using $E_i=355$ meV are described less accurately because the energy resolution is lower, but the high-energy cutoff is still determined correctly (Fig. 4). To outline the higher band of optical bond-stretching D vibrations in the NERA-PR spectrum of AlD$_3$ shown in Fig. 2(a), we fitted this spectrum with the HRMECS spectrum of AlH$_3$ (Fig. 4, curve for $E_i=355$ meV), transformed to $G(E)$, and rescaled along the E axis to get the same high-energy cutoff near 96 meV of the band of bond-bending vibrations. The result of the fitting is presented in Fig. 6. The optimum scaling factor of 1.35 is close to that of 1.37 used to fit the optical part of the spectrum of AlD$_3$ with the NERA-PR spectrum of AlH$_3$ [Fig. 2(b)].

As seen from Fig. 6, the peaks near 154 and 175 meV in the spectrum of AlD$_3$ definitely originate from the stretching
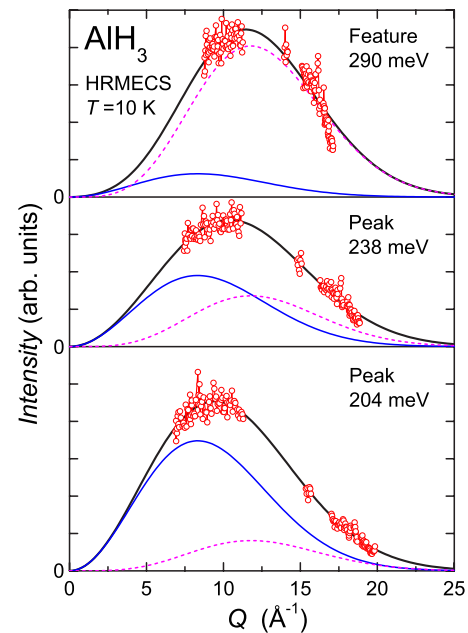
FIG. 5. (Color online) The integral intensities of the peaks at 204 and 238 meV and the spectral area around 290 meV in the $S(Q,E)$ spectrum of AlH$_3$ (see Fig. 4) plotted as a function of neutron momentum transfer. The open circles show the experimental data collected at 10 K with the HRMECS. The solid line fitting each set of the experimental data is a sum of the one-phonon (lower solid line) and two-phonon (dashed line) scattering contributions calculated by using Eq. (2).

modes. These peaks are better seen in the spectrum of AlD$_3$ than in the spectrum of AlH$_3$ measured with the same spectrometer NERA-PR because of the less exterminative effect of the Debye-Waller factor, $\exp(-\langle u^2 \rangle Q^2)$. This factor is larger for the vibrations in AlD$_3$ because they are excited at smaller energy and, correspondingly, smaller momentum
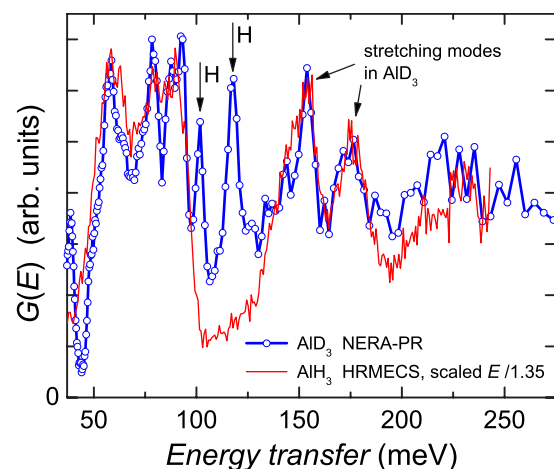
FIG. 6. (Color online) The experimental spectrum $G(E)$ of AlD$_3$ measured at 9 K with NERA-PR (open circles connected with the thick solid line) and that of AlH$_3$ measured at 10 K with HRMECS and plotted as a function of $E=E/1.35$ (thin solid line). The two vertical arrows show the peaks from the H impurity in the AlD$_3$ sample.

transfers Q and because the mean-squared displacement $\langle u^2 \rangle$ of the heavier D atoms is smaller.

C. Local vibrations of H impurity atoms in AlD$_3$

The fitting of the experimental $G(E)$ spectrum of AlD$_3$ with the rescaled spectra of AlH$_3$ measured with both NERA-PR [Fig. 2(b)] and HRMECS (Fig. 6) showed the occurrence of two peaks positioned at 101.5 and 117.5 meV and resulting from vibrations of 1.5% hydrogen impurity atoms contained in the studied AlD$_3$ sample. In order to substantiate that these two peaks arise from local transverse modes of the H defects and that these defects do not disturb the phonon density distribution in the ranges of optical bands of AlD$_3$, we performed lattice dynamics simulations of the experimental spectra of AlD$_3$ and AlH$_3$ samples measured with NERA-PR.

Hydrogen defect modes were earlier observed and studied by INS in a few metal deuterides, e.g., PdD$_{0.125}$H$_{0.005}$ (Ref. 10) and β-YD$_{2-x}$H$_x$ (Ref. 11). In all these deuterides, the H atoms were on positions with cubic symmetry that gave rise to a triple degenerate vibrational mode. In a deuteride like AlD$_3$ with a lower symmetry of D positions that are partly occupied by atoms of the H impurity, an isolated H defect has three nondegenerate normal vibrational modes with three different energies. Despite the absence of translational symmetry, the lattice dynamics of such an isotopically dilute solid solution can be accurately calculated by traditional methods developed for periodical structures. Usually, the problem is solved for a periodic structure, in which one impurity atom is placed in a unit cell of the deuteride and the cell is chosen large enough to neglect the interaction among the impurity atoms in different cells. If the H-H interaction is weak, a reasonably good solution can be produced for a finite concentration of H defects by using a smaller unit cell. For example, the Born–von Kármán model was successfully applied[12] to calculate the H defect modes in D$_2$O ice-Ih by placing one H atom in the standard unit cell of ice-Ih composed of four molecules of heavy water that corresponded to the composition D$_7$HO$_4$.

In the present work, we applied the Born–von Kármán model to solve the lattice dynamics of the pure AlH$_3$ and AlD$_3$ compounds using a reduced unit cell containing 3 f.u. and the lattice dynamics of the Al$_3$D$_8$H compound with one D atom substituted by a H atom in the same reduced unit cell. The calculation showed that the presence of one H atom (11.1% H impurity) in the unit cell of Al$_3$D$_8$H did not lead to any noticeable changes in the phonon density of states of the remaining eight D atoms compared to the case of pure AlD$_3$. We therefore concluded that the contributions from vibrations of the H and D atoms are additive at H concentrations of up to 11% at least, so we composed the phonon spectrum of our AlD$_3$ sample containing 1.5% H impurity by using the H and D contributions calculated for the Al$_3$D$_8$H compound and taken in the proper ratio.

The lattice dynamics calculations were carried out using the UNISOFT code.[13] The longitudinal central forces between the nearest atoms only were taken into account. The H-H interaction in the simulative Al$_3$D$_8$H compound was ne-
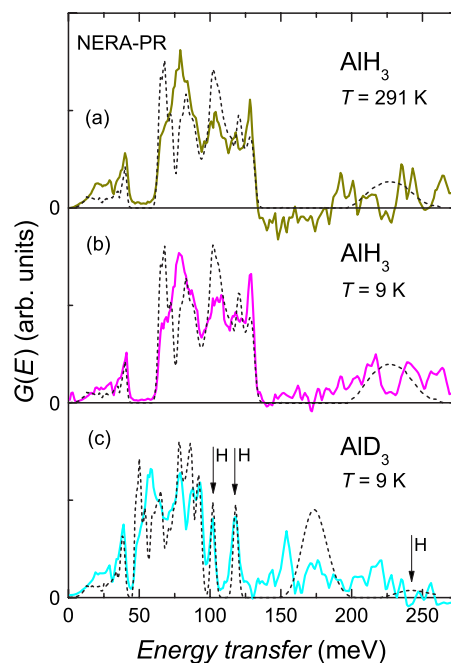
FIG. 7. (Color online) The solid curves show the one-phonon experimental $G(E)$ spectra of the AlH$_3$ and AlD$_3$ samples measured with NERA-PR. The dashed curves present the $G(E)$ spectra calculated in the Born–von Kármán model using the force constants listed in Table I and convoluted with the NERA-PR resolution function. The vertical arrows in (c) indicate the calculated peaks of three local vibrational modes of the H impurity in the AlD$_3$ sample.

glected assuming a large mean distance between the nearest H impurity atoms. All other longitudinal force constants served as fitting parameters.

The generalized vibrational density of phonon states was calculated as a sum of partial densities:

$$G_i(\omega) = \frac{f_i \sigma_i^{\text{tot}}}{3 N m_i} \exp(-\langle u^2 \rangle Q^2) \sum_{j,\mathbf{q}} |\mathbf{e}(i|\mathbf{q}j)|^2 \delta[E - E_j(\mathbf{q})],$$

(3)

where $E_j(\mathbf{q})$ and $\mathbf{e}(i|\mathbf{q}j)$ are the eigenvalues and eigenvectors of the dynamical matrix corresponding to the phonon state $\mathbf{q}j$, while m_i, σ_i^{tot}, and f_i are the mass, total neutron scattering cross section, and concentration of atom i. The summation in Eq. (3) ran over $N = 1000$ points in $\mathbf{q}$ space, uniformly distributed over the reduced Brillouin zone. The calculated spectrum was convoluted with the NERA-PR resolution function and compared with the corresponding experimental one-phonon spectrum. The fitting parameters were then optimized using a trial-and-error method so as to reproduce the high-energy cutoff of the experimental band of lattice vibrations and also the low-energy and high-energy cutoffs of the lower optical band of bond-bending vibrations.

Figure 7 shows the calculated spectra together with the experimental ones. The optimum values of the force constants are listed in Table I. As one can see, the model provides a satisfactory fit of the lattice band and lower optical band in the spectra of both AlH$_3$ and AlD$_3$ samples using similar values of the force constants. Moreover, the positions

TABLE I. Longitudinal force constants L (in N/m) used in the Born–von Kármán model calculations.

Real sample	Composition in calculations	L(Al-Al)	L(Al-H)	L(Al-D)	L(H-H)	L(D-D)	L(H-D)
AlH$_3$	AlH$_3$	24	90		8.4		
AlD$_{2.955}$H$_{0.045}$	AlD$_{8/3}$H$_{1/3}$	24	103	106	0	8.8	8.2

and intensities of the two peaks at 101.5 and 117.5 meV in the spectrum of the AlD$_3$ sample are well reproduced as resulting from two transverse H defect modes [Fig. 7(c)]. This suggests that the model is adequate and the peak assignments are correct.

As seen from Fig. 7, the fitting of the higher optical band of bond-stretching vibrations is not very accurate. Nevertheless, the model still satisfactorily outlines the energy span of this band in the spectra of both AlH$_3$ and AlD$_3$. We can therefore expect that the energy of 220–260 meV of the bond-stretching H defect mode [Fig. 7(c)] is also estimated reliably and this mode lies far beyond the energy intervals of optical vibrations of the D atoms.

D. Phonon densities of states of AlH$_3$ and AlD$_3$

The results obtained with the NERA-PR spectrometer and HRMECS made it possible to construct the entire spectrum of one-phonon generalized vibrational density of states, $G(E)$, for α-AlH$_3$ and also for α-AlD$_3$. To get the spectrum $g(E)$ of phonon density of states, the one-phonon $G(E)$ spectrum was divided by the Debye-Waller factor, separated into nonoverlapping bands of lattice vibrations and two optical bands, and finally, each of these three bands was normalized to represent the number of corresponding phonon modes (6, 12, and 6 modes, respectively[3]). The $g(E)$ spectra of AlH$_3$ and AlD$_3$ produced in this way are shown in Fig. 8 together with the spectrum of AlH$_3$ calculated in Ref. 3. As one can see, the agreement between the two spectra of AlH$_3$ is good. This suggests that the theoretical calculation[3] and the procedure we used to get $g(E)$ from the experimental INS data are both adequate. More details of the procedure are considered below.

The one-phonon $G(E)$ spectrum of AlH$_3$ was composed of the lattice part (5–46 meV) and lower-energy optical part (60–135 meV) measured at 9 K with NERA-PR [Fig. 1(b)] and the higher-energy optical part (173–263 meV) measured at 10 K with HRMECS using E_i=355 meV. At energies below 5 meV, the spectrum was interpolated using the Debye approximation $G(E) \propto E^2$ as shown in Fig. 3. The one-phonon $S(Q,E)$ spectrum of the higher optical band was obtained from the experimental HRMECS spectrum (Fig. 4) by subtracting the calculated multiphonon contribution. The integral intensities of the two one-phonon peaks thus constructed agreed with the intensities resulted from the analysis of the momentum transfer dependences (Fig. 5). The $S(Q,E)$ spectrum of the higher optical band was then transformed to the $G(E)$ spectrum using Eq. (1).

Each of the three parts of the $G(E)$ spectrum of AlH$_3$ was corrected for the Debye-Waller factor, $\exp(-\langle u^2 \rangle Q^2)$, using

the value $\langle u^2 \rangle$=0.010 Å^2 of the mean-square displacement of H atoms determined while calculating the one-phonon contribution to the INS spectrum measured with NERA-PR [thin solid line in Fig. 1(b)]. This value is close to $c \equiv \langle u^2 \rangle \approx 0.013$ Å^2 resulted from fitting the momentum transfer dependences of scattering intensities in the HRMECS spectrum (Fig. 5) with Eq. (2). Looking through the calculations of one-phonon contribution to the INS spectrum of AlH$_3$ measured at 25 K with the TFXA spectrometer in our previous work,[2] we also found a similar value of $\langle u^2 \rangle$=0.011 Å^2. We must admit in this connection that $\langle u^2 \rangle$=0.024 Å^2 indicated in Ref. 2 was a misprint.

The one-phonon $G(E)$ spectrum of AlD$_3$ was composed of the lattice part (5–43.5 meV), the lower-energy optical
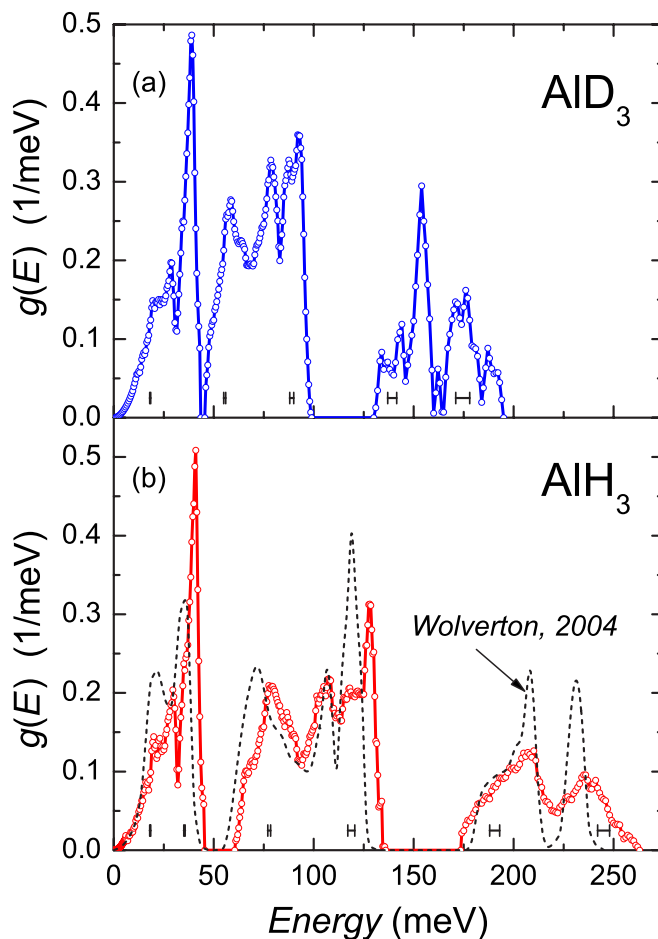
FIG. 8. (Color online) The densities $g(E)$ of phonon states of (a) AlD$_3$ and (b) AlH$_3$ obtained from the INS data (solid curves with open circles) and the phonon density of states calculated for α-AlH$_3$ in Ref. 3 (dashed curve). The horizontal bars show the energy resolution of the INS data.

part (45.5–99 meV), and the higher-energy optical part (130–195 meV) of the spectrum measured at 9 K with NERA-PR [thin solid line in Fig. 2(a)]. Below 5 meV, the spectrum was interpolated using the Debye approximation (Fig. 3). The energy interval 130–195 meV of the higher-energy optical band was estimated from the HRMECS spectrum of AlH$_3$ rescaled along the E axis to reproduce the high-energy cutoff of the lower-energy optical band of AlD$_3$ (Fig. 6). The obtained one-phonon $G(E)$ spectrum of AlD$_3$ was divided by the Debye-Waller factor with $\langle u^2 \rangle$ =0.008 Å^2 derived from the calculation of the one-phonon contribution [thin solid line in Fig. 2(a)].

Further normalization of each part of the spectra of AlH$_3$ and AlD$_3$ to the number of corresponding vibrational modes followed from the usual assumptions[14] that $g(E) \propto G(E)$ in the lattice part of the spectrum and that the squares of the hydrogen eigenvectors of the lattice and optical modes are different but energy independent.

IV. SUMMARY

Finding the high-energy band of optical bond-stretching vibrations and its examination with a good resolution and statistical accuracy (Fig. 4) completed the primary experimental investigations into the lattice dynamics of the α-AlH$_3$ hydride. Combined with the results of studies of the lower-energy vibrational states, this allowed a rather detailed and accurate reconstruction of the phonon density of states in the hydride [Fig. 8(b)]. The INS investigation of AlH$_3$ at two significantly different temperatures of 9 and 291 K demonstrated a harmonic behavior of the low-energy lattice modes and also of the rotational and bond-bending vibrations that form the lower optical band.

The comparative analysis of the INS spectra of the α-AlD$_3$ and α-AlH$_3$ samples made it possible to reliably identify the band of lattice modes and two optical bands in the vibrational spectrum of the AlD$_3$ compound. The phonon density of states in α-AlD$_3$ was reconstructed in the ranges of two lower bands and estimated rather plausibly for the high-energy optical band [Fig. 8(a)]. The low-energy lattice modes, which are mostly governed by movements of the heavy Al atoms, virtually showed a harmonic behavior with respect to the isotopic substitution of H by D. In going from AlH$_3$ to AlD$_3$, the energies of all modes of the lower optical band decreased by a factor of 1.37 that was smaller than the harmonic factor $\sqrt{m_D/m_H} \approx \sqrt{2}$ for the vibrating atoms and therefore suggested stronger D-Al force constants compared to the H-Al ones. The effect may partly be due to the smaller interatomic distances in AlD$_3$.

The AlD$_3$ sample contained 1.5% H impurity atoms that manifested themselves by two peaks at 101.5 and 117.5 meV in the INS spectrum. Simulating the spectrum in the Born–von Kármán model identified the peaks as resulting from two transverse H defect modes. This suggests that most H atoms were randomly distributed over the sample volume and formed individual structure defects.

*akolesnikov@anl.gov

[1] J. W. Turley and H. W. Rinn, Inorg. Chem. **8**, 18 (1969).

[2] A. I. Kolesnikov, M. Adams, V. E. Antonov, N. A. Chirin, E. A. Goremychkin, Yu. E. Markushkin, M. Prager, and I. L. Sashin, J. Phys.: Condens. Matter **8**, 2529 (1996).

[3] C. Wolverton, V. Ozoliņš, and M. Asta, Phys. Rev. B **69**, 144109 (2004).

[4] X. Ke, A. Kuwabara, and I. Tanaka, Phys. Rev. B **71**, 184107 (2005).

[5] F. M. Brower, N. E. Matzek, P. F. Reigler, H. W. Rinn, C. B. Roberts, D. L. Schmidt, J. A. Snover, and K. Terada, J. Am. Chem. Soc. **98**, 2450 (1976).

[6] C.-K. Loong, S. Ikeda, and J. M. Carpenter, Nucl. Instrum. Methods Phys. Res. A **260**, 381 (1987).

[7] I. Natkaniec, S. I. Bragin, J. Brankowski, and J. Mayer, ICANS-XII, RAL Report 94–025, 1994, Vol. 1, p. 89; http://nfdfn.jinr.ru/fks/nerapr.html.

[8] A. I. Kolesnikov, I. Natkaniec, V. E. Antonov, I. T. Belash, V. K. Fedotov, J. Krawczyk, J. Mayer, and E. G. Ponyatovsky, Physica B **174**, 257 (1991).

[9] V. F. Sears, Neutron News **3**, 26 (1992).

[10] J. J. Rush, J. M. Rowe, and D. Richter, Phys. Rev. B **31**, 6102 (1985).

[11] T. J. Udovic, J. J. Rush, and I. S. Anderson, Phys. Rev. B **50**, 15739 (1994).

[12] J.-C. Li and D. K. Ross, J. Phys.: Condens. Matter **6**, 10823 (1994).

[13] G. Eckold, M. Stein-Arsic, and H.-J. Weber, *UNISOFT–A Program Package for Lattice-Dynamics Calculations: User Manual* (Jülich, IFF KFA, 1986), Jül-Spez-366.

[14] T. Springer and D. Richter, *Methods of Experimental Physics*, edited by K. Sköld and D. Price (Academic, New York, 1987), p. 131.